Photoaffinity Labeling of the Human Receptor for Urokinase-Type Plasminogen Activator Using a Decapeptide Antagonist. Evidence for a Composite Ligand-Binding Site and a Short Interdomain Separation†

Michael Ploug,*,‡ Søren Østergaard,§,|| Lars Bo Laurenborg Hansen,‡ Arne Holm,§ and Keld Danø‡

Finsen Laboratory, Rigshospitalet, Strandboulevarden 49, DK-2100 Copenhagen Ø, Denmark and Chemistry Department, Royal Veterinary and Agricultural University, Thorvaldsensvej 40, DK-1871 Fredriksberg C, Denmark

Received November 12, 1997; Revised Manuscript Received January 14, 1998

ABSTRACT: Binding of urokinase-type plasminogen activator (uPA) to its cellular receptor (uPAR) renders the cell surface a favored site for plasminogen activation. Recently, a 15-mer peptide antagonist of the uPA−uPAR interaction, with an IC_{50} value of 10 nM, was identified using phage display technology [Goodson, R. J., Doyle, M. V., Kaufman, S. E., and Rosenberg, S. (1994) *Proc. Natl. Acad. Sci. 91*, 7129−7133]. In the present study, the molecular aspects of the interaction between this peptide and uPAR have been investigated. We have characterized the real-time receptor binding kinetics for the antagonist using surface plasmon resonance and identified critical residues by alanine replacements. The minimal peptide antagonist thus derived (SLNFSQYLWS) was rendered photoactivatable by replacing residues important for uPAR binding with photochemically active derivatives of phenylalanine containing either (trifluoromethyl)diazirine or benzophenone. These peptides incorporated covalently into purified soluble uPAR upon photoactivation, and this was inhibited by preincubation with receptor binding derivatives of uPA. The intact three-domain structure of uPAR was essential for efficient photoaffinity labeling. Proteolytic domain mapping using chymotrypsin revealed a specific labeling of both uPAR domain I and domains II + III dependent on the position of the photoprobe in the antagonist. On the basis of these studies, we propose the existence of a composite ligand binding site in uPAR combined of residues located in distinct structural domains. According to this model, a close spatial proximity between uPAR domain I and either domains II or III in intact uPAR is required for the assembly of this composite binding site. Since the receptor binding properties of the peptide antagonist closely mimic those of uPA itself, these two ligands presumably share a coincident binding site in uPAR.

Urokinase-type plasminogen activator (uPA)[1] is one of two modular serine proteases dedicated to the proteolytic conversion of the abundant proenzyme plasminogen to plasmin, which has a well-established role in thrombolysis (*1*). An additional role for plasminogen activation in tissue remodeling during tumor invasion and wound healing has also been implicated (*2, 3*). Several in vivo stimulated cell types involved in such pathological conditions, e.g., differentiated monocytes, activated neutrophiles, migrating keratinocytes, and certain types of cancer cells (*4*−*7*), demonstrate an increased level in their surface expression of a membrane glycoprotein, which binds uPA with high affinity ($K_d \approx 0.1-1$ nM). Confinement of uPA to the plasma membrane via specific interaction with this uPA receptor (uPAR) renders the cell surface a kinetically favored microenvironment for uPA-mediated plasminogen activation (*8*). Several investigations employing experimental in vivo model systems implicate receptor-bound uPA in the process of cancer invasion and metastasis (*9*−*15*). Consequently, the specific interaction between uPA and uPAR represents an attractive target for the development of low molecular weight binding antagonists with potential applications for cancer therapy.

Nascent human uPAR is encoded as a single polypeptide chain of 313 amino acids (*16*), but approximately 30 residues are excised from its COOH-terminus during the posttranlational addition of a glycolipid anchor (*17*). The uPA receptor is thus entirely extracellular, since its attachment to the plasma membrane exclusively is mediated via the embedment of a COOH-terminal glycosyl-phosphatidylinositol moiety in the outer leaflet of the lipid bilayer (*17*). The entire protein sequence of fully processed uPAR consists of three consecutive Ly6/uPAR-type domains[2] separated by long interdomain linker sequences (*18*−*20*). All members belonging to this

† This work was supported financially by the Danish Cancer Society and Dansk Kræftforsknings Fond.

* To whom correspondence should be addressed. Tel: +45-35455708. Fax: +45-35385450. E-mail: m-ploug@finsenlab.dk.

‡ Finsen Laboratory.

§ Royal Veterinary and Agricultural University.

|| Present address: Dept. Insulin Research, NOVO-Nordisk A/S, Novo Allé 6B, DK-2880 Bagsværd, Denmark.

[1] Abbreviations: ANS, 8-anilino-1-naphthalene sulfonate; ATF, amino terminal fragment of uPA; BIA: biospecific interaction analysis; Bpa: *p*-benzoyl-L-phenylalanine; DSS: N,N'-disuccinimidylsuberate; Fmoc: 9-fluorenylmethoxycarbonyl; GFD: growth factor-like domain of uPA; MALDI-MS: matrix-assisted laser desorption ionization mass spectrometry; (Tmd)Phe: 3-[*p*-(trifluoromethyl)-3H-diazirine-3-yl]-L-phenylalanine; uPA: urokinase-type plasminogen activator; uPAR: uPA receptor; suPAR: soluble recombinant uPAR;

[2] Recommended nomenclature as proposed by Bork, P., & Bairoch, A. (1995) *Trends Biochem. Sci. 20* (3), poster C02.

S0006-2960(97)02787-6 CCC: $15.00
Published on Web 02/25/1998

Ly6/uPAR superfamily are glycolipid anchored-membrane glycoproteins and all except uPAR are single domain proteins, typified by the complement regulatory protein CD59. Although no experimental three-dimensional protein structure as yet is available for human uPAR, its three individual domains are thought to adopt an overall folding topology similar to that solved for human CD59 (*20*−*22*). Biochemical studies of ligand binding are conveniently performed with a recombinant, soluble uPAR (denoted suPAR), which is secreted from transfected cells due to a genetic deletion of the COOH-terminal signal sequence responsible for the glycolipid modification. This recombinant suPAR (residues 1−277) resembles a soluble uPAR secreted in vivo from peripheral blood cells affected by the acquired stem cell disease paroxysmal nocturnal hemoglobinuria (*23*, *24*) and has an equilibrium binding constant for uPA, which is indistinguishable from that of the natural, glycolipid-anchored uPAR present on cells (*25*).

Although the structural elements required for the high-affinity interaction between uPA and uPAR primarily resides within the small ω-loop of the growth factor like module of uPA (*26*−*29*), the assembly of an intact, high-affinity ligand binding site in uPAR appears much more complex. The NH_2-terminal domain I of uPAR (residues 1−87) has the primary role in uPA binding as demonstrated by chemical cross-linking and a protein−protein footprinting analysis (*18*, *28*). However, the integrity of the multidomain structure of uPAR is required for maintenance of the high-affinity binding site for uPA (*20*, *30*). Furthermore, the availability of a surface-exposed hydrophobic patch on uPAR detected by ANS fluorescence is directly related to the unoccupied, high-affinity ligand-binding conformation of uPAR (*20*).

To further elucidate structural aspects important for the receptor−ligand interaction we have now characterized the real-time binding kinetics of a uPAR binding peptide antagonist selected by bacteriophage display technology (*31*). The functional key residues of this peptide were identified by alanine replacements revealing the presence of two distinct functional sites. Truncated derivatives of this peptide containing photochemical analogues of phenylalanine (i.e., benzophenone or (trifluoromethyl)diazirine) were used to obtain a specific, site-directed photoaffinity labeling of the ligand-binding site in purified three-domain uPAR. These studies reveal that the receptor recognition sites, corresponding to the two distinct functional regions of the peptide antagonist, are located on separate domains of uPAR. Information derived from such topological mapping experiments of the receptor−ligand interface may provide the structural basis for a focused site-directed mutagenesis analysis of the uPA binding determinants in uPAR and may furthermore be useful for future rational refinements of existing receptor−ligand antagonists.

MATERIALS AND METHODS

Chemicals and Reagents. N^{α}-(9-Fluorenylmethoxycarbonyl) (Fmoc)-protected amino acids were from either Perseptive or Novabiochem (La Jolla, CA). Trityl was used as side-chain protecting group for Asn, Gln, and His, *tert*-butyl was used for Tyr, Ser, Thr, and Glu, while *tert*-butyloxycarbonyl was used for Trp. Fmoc-protected *p*-benzoyl-L-phenylalanine (Bpa) was purchased from Bachem (Bubendorf, Switzerland). KA-resins (Novasyn KA) with preloaded Fmoc-amino acid were purchased from Novabiochem. Bolton-Hunter reagent (*N*-succinimidyl 3-(4-hydroxy-5-[^{125}I]-iodophenyl)propionate) was purchased from Amersham (Buckinghamshire, U.K). Water was drawn from a Milli-Q system with an Organex-Q cartridge.

Synthesis of 3-[p-(Trifluoromethyl)-3H-diazirin-3-yl]-L-phenylalanine. The synthesis of 3-[*p*-(trifluoromethyl)-3*H*-diazirin-3-yl]-L-phenylalanine [(Tmd)Phe] was performed in 14 steps according to Nassal (*32*) including minor refinements (*33*, *34*): α_D +17.5° (*c* 1.21) in DMSO containing 2% TFA; mp 180−200 °C dec; 300 MHz ^{1}H NMR (DMSO d_6) δ 8.5 (br s, 2.2H), 7.44 (d, 2H), 7.24 (d, 2H), 4.18 (br t, 1H), 3.20 (d, 2H).

Synthesis of N-(9-Flourenylmethoxycarbonyl)-3-[p-(trifluoromethyl)-3H-diazirin-3-yl]-L-phenylalanine (Fmoc-(Tmd)Phe-OH). The Fmoc acylation of (Tmd)Phe was carried out essentially as described (*35*). The Fmoc-(Tmd)-Phe-OH thus synthesized was recovered with an overall yield of 85% starting from 2 g of Tmd(Phe) and consisted of colorless crystals: mp 121−2 °C; R_f = 0.40 ethyl acetate/methanol (2:1); 300 MHz ^{1}H NMR ($CDCl_3$ + 5% DMSO-d_6) δ 7.77d (2H), 7.56 dd (2H), 7.40 t (2H), 7.28 t (2H), 7.18 (br d, 2H), 7.04 (br d, 2H), 5.65 (br d, NH, 1H), 4.57 (dd, 1H), 4.47 (dd, 1H), 4.31 (dd, 1H), 4.18 (m, 1H), 3.23 (dd, 1H), 3.09 (dd, 1H).

Peptide Synthesis. The chain-elongation steps of the solid-phase peptide synthesis were carried out manually using polyethylene syringes as reaction vessels. Synthesis was performed on KA-resin with preloaded Fmoc-amino acids on an acid-labile linker. Five equivalents of Fmoc-amino acids activated by 1-hydroxy-7-azabenzotriazole and *N*,*N*′-diisopropylcarbodiimide were used in the coupling steps and were allowed to react for more than 2 h. Fmoc-(Tmd)Phe-OH was, however, consequently coupled overnight. The Fmoc protecting group was removed with 20% piperidine in dimethylformamide for 15−20 min. For cleavage, peptide−resins were treated for 1.5 h with 85% TFA containing 5% of phenol, mercaptoethanol, and thioanisole, respectively. The filtrates were concentrated by nitrogen flushing, and peptides were subsequently precipitated from, and washed four times with, diethyl ether. Peptides were finally dissolved/suspended in glacial acetic acid, lyophilized, redissolved in 10% acetic acid, and lyophilized again. Analytical HPLC analysis was performed on a C18 column using Waters 600E equipped with Waters photodiode array detector. A 25 min linear gradient from buffer A (0.1% TFA in H_2O) to 70% buffer B (0.1% TFA, 9.9% H_2O, 90% CH_3-CN) was used. If considered necessary peptides were purified on a preparative scale. The correct identities of the peptides were confirmed by electrospray ionization mass spectrometry (Table 1).

Since neither lysines nor cysteines are present in any of the prepared photolabile peptide antagonists monoradiolabeled derivatives were obtained by specific conjugation at the α-amino group by addition of ^{125}I-labeled Bolton−Hunter reagent. In brief: 5 μL of DMSO containing 35 nmol of the relevant photolabile peptide was mixed in the dark with 18 μL of Bolton−Hunter reagent in dry benzene (containing approximately 90 μCi and 45 pmol of active *N*-hydroxysuccinimide ester). After 5 min, 100 μL of 50 mM phosphate (pH 7.4) was added, and the resultant suspension was

Table 1: Amino Acid Sequence of Synthetic Peptide Antagonists and Their Corresponding Photolabile Analogues

code	sequence	theoretical mass[a] (Da)	determined mass[b] (Da)
AE78	AEPMPHSLNFSQYLWYT	2082.95	2083.6
AE79	AEWSNLMQPYYPSTHFL	2082.95	2083.6
AE68	SLNFSQYLWS	1243.59	1243.7
uPA_{19-31}	CVSNKYFSNIHWC	1597.68	1597.6
AE88	S-***(Tmd)Phe***-NFSQYLWS	1385.57	1385.5
AE81	SLN-***Bpa***-SQYLWS	1347.61	1347.7
AE84	SLN-***(Tmd)Phe***-SQYLWS	1351.58	1351.6
AE86	SLNFSQ-***(Tmd)Phe***-LWS	1335.59	1335.4
AE87	SLNFSQY-***(Tmd)Phe***-WS	1385.57	1385.6
AE83	SLNFSQYL-***Bpa***-S	1308.60	1308.8

[a] The theoretical monoisotopic peptide masses were calculated using the program GPMAW version 3.03 (Lighthouse Data, Odense, Denmark). [b] The molecular masses of these peptides were determined by electrospray ionization mass spectrometry. The mass equivalent to one proton has been subtracted from the recorded *m*/*z* representing the monoisotopic MH^+.

vortexed vigorously at intervals of 5 min during a 30 min incubation in the dark at room temperature. Finally, the suspension was diluted with 400 μL of 0.1 M NH_4HCO_3 to quench any residual active Bolton−Hunter reagent. After these manipulations the peptides retained solubility as judged macroscopically.

Purified Proteins. A soluble recombinant variant of uPAR (residues 1−277) was expressed in Chinese hamster ovary ($dhfr^-$) cells. The suPAR protein was purified by immunoaffinity chromatography using an anti-uPAR monoclonal antibody (*19*). Highly purified suPAR domain II + III (residues 88−277) was generated by limited proteolysis using chymotrypsin and isolated by immunoaffinity chromatography and gel filtration as described previously (*25*). Recombinant human pro-uPA expressed in *E. coli* was generously provided by Dr. D. Saunders (Grünenthal, Germany), and the amino-terminal-fragment (ATF) of uPA was kindly provided by Drs. A. Mazar and J. Henkin (Abbott Laboratories, IL). The growth factor-like domain (GFD) of uPA was produced by endoproteinase Glu-C digestion of recombinant pro-uPA as described previously (*28*). Murine anti-uPAR monoclonal antibodies were either produced at the Finsen Laboratory (clones R2−R9) as described previously (*36*) or at Boehringer Mannheim (Penzberg, Germany) by Drs. U. Weidle and C. Hartle, from whom they were obtained as generous gifts (clones C8.26.A3 and H2.10.A3).

N-Tosyl-L-phenylalanine chloromethyl ketone treated α-chymotrypsin (EC 3.4.21.1) was purchased from Worthington (Freehold, NJ), and a special quality of neuraminidase (EC 3.2.1.18) isolated from *Clostridium perfringens* with low protease contamination was obtained from Boehringer Mannheim (Germany).

Photoaffinity Labeling of uPAR. Photoincorporations were performed in 100 μL aliquots containing 2−10 μM suPAR and equimolar amounts of the relevant ^{125}I-labeled photoactive peptide dissolved in 50 mM phosphate, 150 mM NaCl pH 7.4. Photoactivation of samples was carried out for 45 min in polystyrene dishes (Nunc 96-well dishes) placed on ice with the relevant wells uniformly positioned 1−2 cm from the light source (Philips TL/09 actinic lamp, 20 W, λ_{max} 355 nm).

Real-Time Biomolecular Interaction Analysis (BIA). Association rate constants (k_{assoc}), dissociation rate constants (k_{diss}), and equilibrium binding constants (K_d) for various synthetic peptides and receptor binding derivatives of uPA were determined by surface plasmon resonance (*37*) using a BIAcore2000 instrument (Pharmacia Biosensor, Uppsala, Sweden). Due to the isoelectric point of uPAR (pI ∼ 4.5), terminal sialic acid residues were removed from its N-linked carbohydrates to facilitate chemical immobilization on the sensor chip. This was accomplished by incubating purified suPAR or suPAR domain II + III (1 mg/mL in 50 mM phosphate, 150 mM NaCl, pH 7.4) with 5 μg/mL neuraminidase for 4 h at 37 °C. Such desialylation did not alter the uPA binding kinetics of intact suPAR (unpublished data). Coupling of the neuraminidase-treated suPAR to a BIAcore sensor chip was achieved by injection of 20 μg/mL suPAR in 10 mM sodium acetate pH 5.0 for 6 min at a flow rate of 5 μL min^{-1} using a carboxymethylated dextran matrix (CM5 sensor chip) preactivated with *N*-hydroxysuccinimide/*N*-ethyl-*N*′-[3-(diethylamino)propyl]carbodiimide according to the manufacturer's recommendations. Approximately 1500−2000 resonance units (RU) were immobilized by this procedure (corresponding to 1−2 ng suPAR/mm^2).

Sensorgrams (RU vs time) were recorded at a flow rate of 10 μL min^{-1} at 5 °C using several different concentrations of the ligand (synthetic peptides, uPA, ATF or GFD) in the range of 10−1000 nM in running buffer (10 mM HEPES, 150 mM NaCl, 3 mM EDTA (pH 7.4) including 0.005% surfactant P-20). The sensor chip was regenerated at the end of each run by injection of 0.1 M acetic acid, 0.5 M NaCl. Data obtained from parallel mock coupled flow cells (subjected to the coupling procedure in the presence of buffer only) served as blank sensorgrams for subtraction of changes in bulk refractive index. The sensorgrams obtained were analyzed by nonlinear least-squares curve fitting using BIAevaluation 2.0 software (Pharmacia Biasensor, Uppsala, Sweden) assuming single-site association and dissociation models.

Chemical Cross-Linking. The ability of various peptides to compete for formation of suPAR·ATF complexes was tested by a chemical cross-linking assay (*38*). Purified suPAR (1 nM) was preincubated with 25 μM peptide for 10 min on ice followed by an additional incubation for 10 min after the addition of 0.5 nM ^{125}I-labeled ATF. These reactions were performed in 10 mM HEPES, 150 mM NaCl, 3 mM EDTA (pH 7.4) including 0.005% surfactant P-20 and a final concentration of 0.5% DMSO (originating from the peptide stock solutions). Complexes between suPAR and ^{125}I-labeled ATF were stabilized covalently by the addition of 1 mM *N*,*N*′-disuccinimidyl suberate (a homobifunctional cross-linker) and subsequently visualized by SDS polyacrylamide gel electrophoresis and autoradiography.

Miscellaneous Analyses. SDS polyacrylamide gel electrophoresis was performed according to Laemmli (*39*) on 12% acrylamide gels. Titration of the suPAR-mediated enhancement of 8-anilino-1-naphthalene sulfonate (ANS) fluorescence by addition of various receptor-binding ligands (synthetic peptides, ATF and GFD) was carried out as described previously (*25*). Electrospray ionization mass spectrometry was performed on a Sciex API III triple quadrupole instrument (Sciex, Thornhill, Canada).

Table 2: Binding Kinetics and Equilibrium Constants for the Receptor−Ligand Interaction between Immobilized uPAR and Various uPA Derivatives as Well as Synthetic Peptide Antagonists[a]

ligand	k_{assoc} (M^{-1} s^{-1})	k_{diss} (s^{-1})	K_d (nM)	B_{max} (RU)	ΔRU/Da	mass (Da)
pro-uPA	3.22×10^5	0.086×10^{-3}	0.27	624.3	0.013	46 399.8
ATF_{6-135}	3.77×10^5	0.105×10^{-3}	0.28	170.1	0.012	14 684.6
GFD_{4-43}	8.33×10^5	0.196×10^{-3}	0.24	36.9	0.008	4464.0
uPA_{19-31}	8.15×10^5	12.0×10^{-3}	14.7	13.9	0.009	1598.8
AE78	6.17×10^5	5.88×10^{-3}	9.5	18.0	0.009	2084.3
AE68	12.8×10^5	24.1×10^{-3}	18.8	7.0	0.005	1244.4
AE79	nd	nd	nd	−0.44	nd	2084.3

[a] Association rate constants (k_{assoc}) and dissociation rate constants (k_{diss}) were determined by surface plasmon resonance analysis using a Biacore2000 equipment as described in the Materials and Methods. Equilibrium dissociation constants were calculated as $K_d = k_{diss}/k_{assoc}$. For the protein ligands (pro-uPA, ATF and GFD) the constants shown were obtained from analysis of 10 nM ligand and for the peptide ligands (uPA_{19-31}, AE68, AE78, and AE79) of 30 nM ligand. Resonance levels measured at high ligand concentrations (100 nM of pro-uPA, ATF, or GFD and 1 μM of the synthetic peptides) were used as approximations of the maximal binding (B_{max}) from which the relative binding stoichiometry for each ligand was derived (ΔRU/Da). Values were read at time point 800 s in Figure 1. The average mass of the various ligands was calculated from their primary sequence using the program GPMAW version 3.03. nd: not determined.

RESULTS

Binding Kinetics and Specificity of the Interactions between Various Ligands and Immobilized suPAR. A number of 15-mer peptides that bind purified suPAR were recently identified by affinity selection from a random peptide library constructed by phage display technology (*31*). Several of these peptides were quite potent antagonists of the uPA−uPAR interaction, the best of which (PMPHSLNFSQYLWYT) exhibited an IC_{50} value of 10 nM, when tested in a competitive ligand-binding ELISA. To study the molecular interaction between this peptide and suPAR in detail, we have synthesized the corresponding 15-mer peptide having an additional two amino acid extension at the NH_2-terminus derived from the vector sequence (denoted AE78, Table 1). The kinetics of its interaction with immobilized suPAR were determined in real time by surface plasmon resonance (Table 2). The equilibrium binding constant (K_d) derived from the measured association and dissociation rates of AE78 was comparable to the IC_{50} value determined previously by competition experiments in an ATF−suPAR ligand-binding ELISA (9.5 vs 10 nM). We also explored the binding properties of a second, putative peptide ligand for suPAR by surface plasmon resonance. A 13-mer synthetic, cyclic peptide (uPA_{19-31}) representing the receptor binding sequence of the growth-factor like module of uPA[3] was also found to associate with immobilized suPAR, but did not retain the high-affinity binding of GFD (Table 2). Since AE78 was superior to the cyclic uPA_{19-31} in terms of receptor affinity, offered more facile synthesis, and allowed the possibility of chain truncation we decided to use AE78 to probe the ligand-binding site in uPAR by photoaffinity labeling.

The interaction of AE78 with immobilized suPAR closely mimics uPA binding and conforms to the following independent criteria of specificity: First, a peptide with a composition identical to AE78, but having its sequence scrambled randomly (AE79), did not exhibit any measurable interaction with immobilized suPAR (Figure 1B). Second, the stoichiometry for the interaction between AE78 and suPAR corresponds to those measured for several other receptor ligands of varying molecular masses (Figure 1A,B; Table 2). Third, no interaction of AE78 with immobilized suPAR domain II + III (residues 88−277) could be measured by surface plasmon resonance (Figure 1C), a finding consistent with the receptor-binding profile for uPA, ATF, and GFD, which exhibit an absolute requirement for the intact multidomain status of uPAR for high-affinity interaction (*25*). Fourth, like uPA and its derivatives, the peptide antagonist AE78 titrates the suPAR-mediated enhancement of 8-anilino-1-naphthalene sulfonate (ANS) fluorescence at a 1:1 molar ratio between uPAR and AE78 (Figure 2). ANS is a low molecular weight fluorophore that reports on the presence of the high-affinity binding site for uPA via interaction with a surface-exposed hydrophobic patch present only on the unoccupied, intact three-domain receptor (*25*). Therefore, by these criteria AE78 represents an appropriate surrogate for uPA in the interaction with uPAR.

Identification of Residues within AE78 Responsible for its Antagonistic Properties. To determine the minimal length of AE78 required to maintain antagonist effect on the uPA−uPAR interaction, we synthesized a number of peptides with sequential two amino acid deletions from either the NH_2-terminus or the COOH-terminus. When these peptides were tested in a chemical cross-linking assay as competitors, it was evident that substantial truncation is allowed at the NH_2-terminus, but not at the COOH-terminus (Figure 3). The decapeptide (AE68: SLNFSQYLWS)[4] was chosen as the minimal antagonist for further structural studies. Surface plasmon resonance analysis revealed that the receptor-binding properties of this peptide were only marginally affected by such truncations compared to the original 17-mer antagonist (Table 2, Figure 1B). To determine the contribution of the individual amino acids of AE68, it was subjected to a systematic alanine scanning, and the resultant peptides were tested as competitors by chemical cross-linking. As shown in Figure 4, alanine replacement of either Leu^2, Phe^4, Leu^8, or Trp^9 abolish the antagonistic property of the decapeptide. In contrast, the remaining alanine substitutions are either without detectable effect (Ser^5, Gln^6, and Ser^{10}) or cause a moderate reduction in efficacy (Ser^1, Asn^3, and Tyr^7). These data therefore indicate that the sequence of the decapeptide (AE68) may contain two distinct regions essential for its antagonistic properties (Figure 4B).

Site-Directed Photoaffinity Labeling of the Ligand-Binding Site in uPAR Using Photoactivatable Analogues of AE68. Having established the specificity and assigned the functional groups of the linear decapeptide antagonist (AE68) a variety of photoactivatable analogues were synthesized (Table 1).

[3] This peptide encompasses all residues of uPA demonstrated to be involved in receptor binding (*28*, *29*) and includes a terminal disulfide bond to restrict the conformational freedom of the peptide. The introduction of this unnatural disulfide seems reasonable upon inspection of the three-dimensional structure of ATF (*27*).

[4] Note that AE68 accidentally was synthesized with a COOH-terminal Ser instead of Tyr, the residue found at the equivalent position in AE78. Fortuitously this replacement was of minor importance since it occurred at a less critical position with respect to the antagonistic properties of the peptide (Figure 4B).

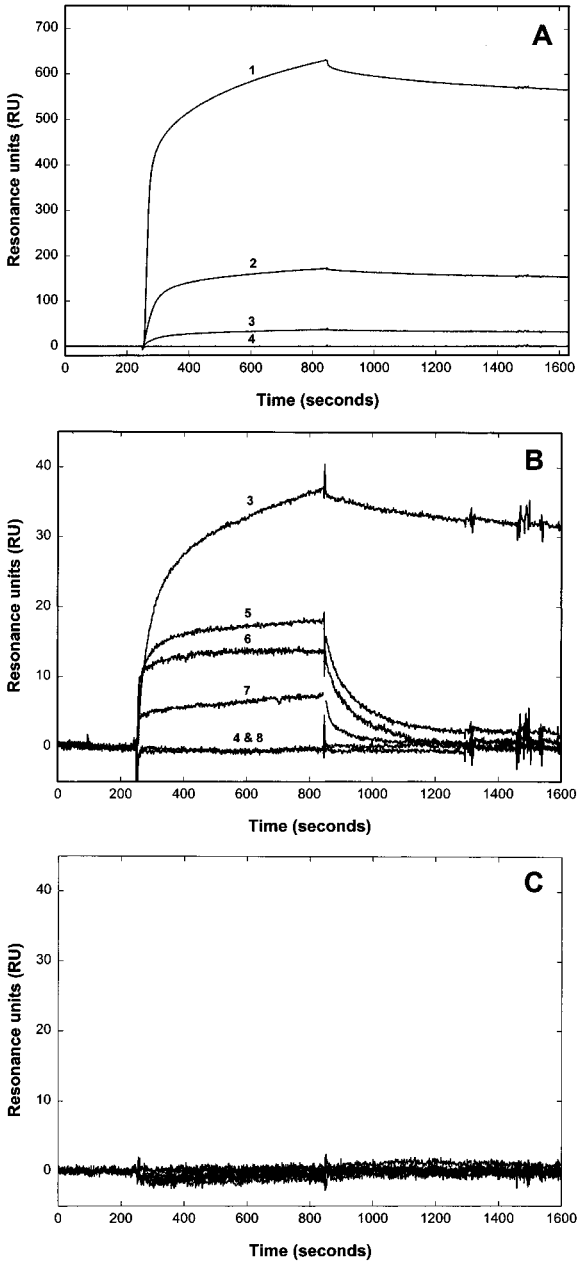

FIGURE 1: Real-time binding curves for the interaction between various ligands and immobilized uPAR measured by surface plasmon resonance. Panel A shows real-time interaction analyses (sensorgrams) recorded on a Biacore2000 for the binding of 100 nM pro-uPA (curve 1), 100 nM ATF (curve 2), and 100 nM GFD (curve 3) to immobilized, neuraminidase-treated suPAR. Also shown is the sensorgram recorded for a buffer control (curve 4). Panel B shows similar sensorgrams recorded for 100 nM GFD (curve 3), 1 μM of the peptide antagonist AE78 (curve 5), 1 μM uPA_{19-31} (a synthetic peptide representing the receptor binding ω-loop of GFD) (curve 6), 1 μM AE68 (a truncated version of AE78) (curve 7), 1 μM of AE79 (a scrambled version of AE78) (curve 8), and a buffer control (curve 4). Panel C shows the sensorgrams recorded for the interactions between immobilized, neuraminidase-treated uPAR domain II + III and either 100 nM pro-uPA, ATF, and GFD or 1 μM the synthetic peptides AE78, AE79, AE68, and uPA_{19-31}. Note that the scaling of the *y*-axis is identical to the one used for the interaction between intact uPAR and the low molecular mass antagonists (panel B), although the present analysis also include the macromolecular ligands pro-uPA, ATF, and GFD. Association of ligands occurred for 600 s by injection of the relevant protein after 250 s of buffer flow. Dissociation was initiated after 850 s. Analyses were performed at a 5 °C with a buffer flow of 10 μL/min.

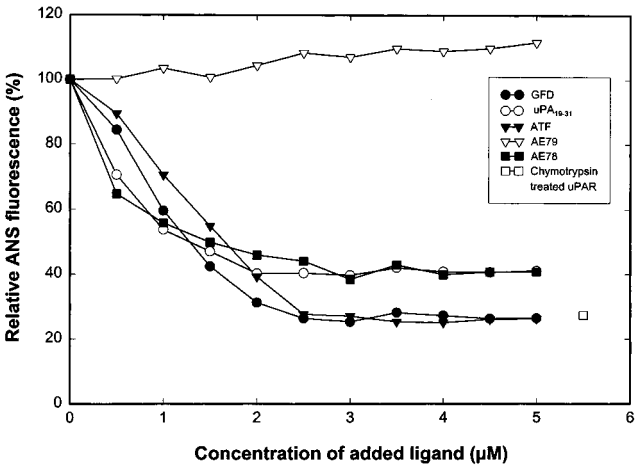

FIGURE 2: Titration of the specific uPAR-mediated enhancement in the quantum yield of ANS fluorescence by various receptor binding ligands. ANS fluorescence was recorded for 2 μM suPAR containing 10 μM ANS and increasing concentrations of the various ligands: ATF (▼), GFD (●), AE78 (■), AE79 (▽), and uPA_{19-31} (○). Also shown is the residual ANS fluorescence of suPAR after chymotrypsin treatment (□) separating domain I (residues 1−87) from domain II + III (residues 88−277), neither of which have high-affinity binding affinities to uPA (25). Excitation and emission wavelengths were 386 and 470 nm, respectively. The ANS profiles shown have been corrected for buffer dilution as well as contributions from intrinsic fluorescence of the individual ligands.

Replacement of key positions in AE68 by photochemically active probes led to a noticeable reduction in the receptor-binding properties of these peptide analogues, in accordance with the outcome of the alanine scanning analysis. These peptides still exhibited a specific interaction with intact suPAR detected by surface plasmon resonance, although the dissociation rates between the photoactive peptides and immobilized suPAR now were too fast to be quantified reliably (data not shown). These photoactivatable peptides were therefore tagged at the α-amino group by conjugation with ^{125}I-labeled Bolton−Hunter reagent and subsequently subjected to photolysis in the presence of equimolar amounts of purified suPAR. As shown in Figure 5, all peptides tested exhibited a specific light-dependent photolabeling of suPAR with incorporation yields ranging from 0.2% to 4.9%. The most prominent photoaffinity labeling of suPAR was observed when either Phe^4 or Trp^9 was substituted with the corresponding photochemical analogues. No appreciable photoadduct formation occurred, if suPAR was preincubated with a 2-fold molar excess of GFD before addition of the photolabile peptides and subsequent photolysis (Figure 6). As these reactions are performed at concentrations (5 μM) far above the equilibrium-binding constant for the interaction between GFD and uPAR ($K_d \approx 0.2$ nM; Table 2), essentially no unoccupied suPAR was available for the peptides during photolysis. This competition experiment therefore demonstrates that specific photolabeling of suPAR requires the exposure of an unoccupied receptor binding site for uPA. Additional competition experiments using other receptor ligands, including pro-uPA, ATF, uPA_{19-31}, and AE78, revealed a similar inhibition of the photolabeling of suPAR, further substantiating the specificity of this site-directed photochemical labeling of a putatively shared interaction site on uPAR (data not shown). Preincubation of suPAR with various anti-uPAR monoclonal antibodies also caused a pronounced reduction in the subsequent photochemical

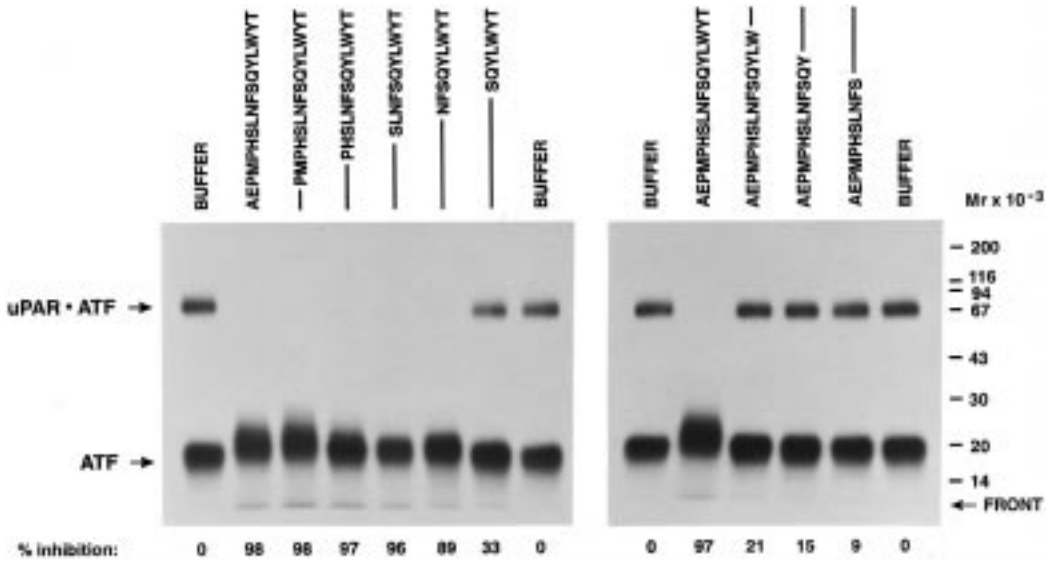

FIGURE 3: Competition of receptor−ligand interaction by truncated versions of the original peptide antagonist probed by chemical cross-linking. Shown are autoradiograms of SDS−polyacrylamide gels (12%) after electrophorectic separations of [^{125}I]-ATF•suPAR complexes formed during a ligand competition assay (see Materials and Methods). Purified suPAR (1 nM) was preincubated with the indicated peptides (25 μM) for 10 min, ^{125}I-labeled ATF was added (0.5 nM), and the resulting [^{125}I]-ATF−suPAR complexes were covalently cross-linked by addition of 1 mM DSS. Samples were reduced and alkylated before SDS−polyacrylamide gel electrophoresis. Buffer controls included 0.5% DMSO. The levels of inhibition were calculated after γ-counting of excised polyacrylamide gel pieces corresponding to ATF•suPAR complexes and are shown at the bottom of the autoradiogram.

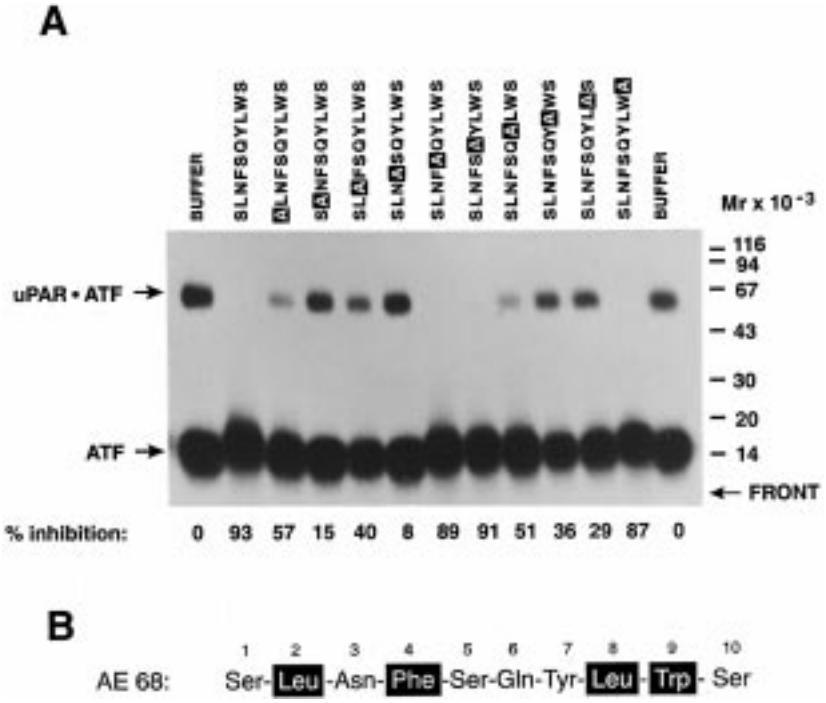

FIGURE 4: Identification of key functional residues in the minimal peptide antagonist analyzed by systematic alanine scanning and chemical cross-linking. Shown in panel A is an autoradiogram of an SDS−polyacrylamide gel (12%) after electrophoretic separation of samples subjected to a ligand competition assay similar to that outlined in the legend to Figure 3. The identity of the peptides used for competition is shown at the top of the autoradiogram with the position of the individual alanine replacements highlighted. The relative inhibitory potentials of these peptides were calculated after γ-counting of excised polyacrylamide gel pieces corresponding to the covalent conjugates formed between suPAR and ATF (shown at the bottom of the autoradiogram). A summary of the conclusion of this experiment is illustrated in panel B, where the key functional residues of AE68 are highlighted.

incorporation of the peptide antagonists if the antibodies in question were inhibitory of the uPA−uPAR interaction (Figure 7). Note that inhibitory antibodies recognizing epitopes on domains II + III also interfered with the covalent photoincorporation of these peptides. One of the monoclonal antibodies (R5), previously recognized as noninhibitory of uPA binding (*25*), appears to affect the photoaffinity labeling of uPAR, but only when AE83 is used as photoprobe (Figure 7). Accordingly, it has recently been demonstrated by surface plasmon resonance studies that R5 actually is a weak, noncompetitive inhibitor of the uPA−uPAR interaction (*40*). An allosteric modulation of the ligand-binding site in uPAR enforced by R5 binding may thus be responsible for the observed selective inhibition of the photoinsertion of AE83

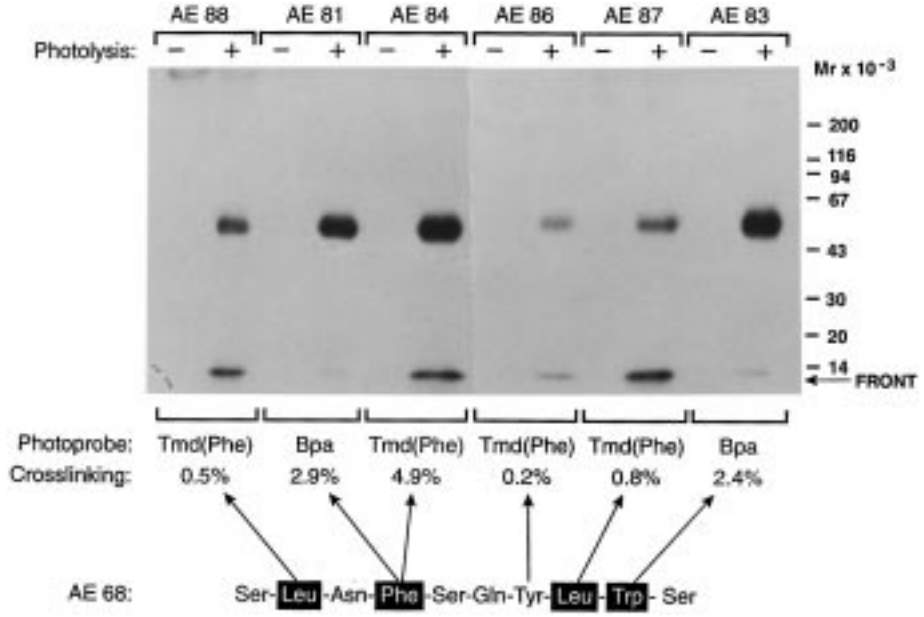

FIGURE 5: Site-directed photoaffinity labeling of purified suPAR using various analogues of AE68. Purified, recombinant suPAR (residues 1−277) was preincubated for 5 min in the dark with an equimolar amount (5 μM) of various photoactivatable analogues of the decapeptide antagonist AE68 (i.e., AE81, AE83, AE84, AE86, AE87, and AE88, see Table 1). One aliquot was subjected to photolysis on ice for 45 min (+), while the other aliquot was incubated in parallel in the dark (−). Finally, these samples were analyzed by SDS−polyacrylamide gel electrophoresis after reduction and alkylation using 20 mM dithiothreitol and 50 mM iodoacetamide, respectively. The corresponding autoradiogram is shown. The photochemical cross-linking yields obtained were determined after excision and (γ-counting of the Coomassie stained bands corresponding to suPAR and was calculated relative to the total amount of radioactivity added. The position and identity of the photoactivatable probe introduced in the various peptide analogues of AE68 is shown at the bottom of the figure. Residues of AE68 critical for uPAR binding are highlighted.

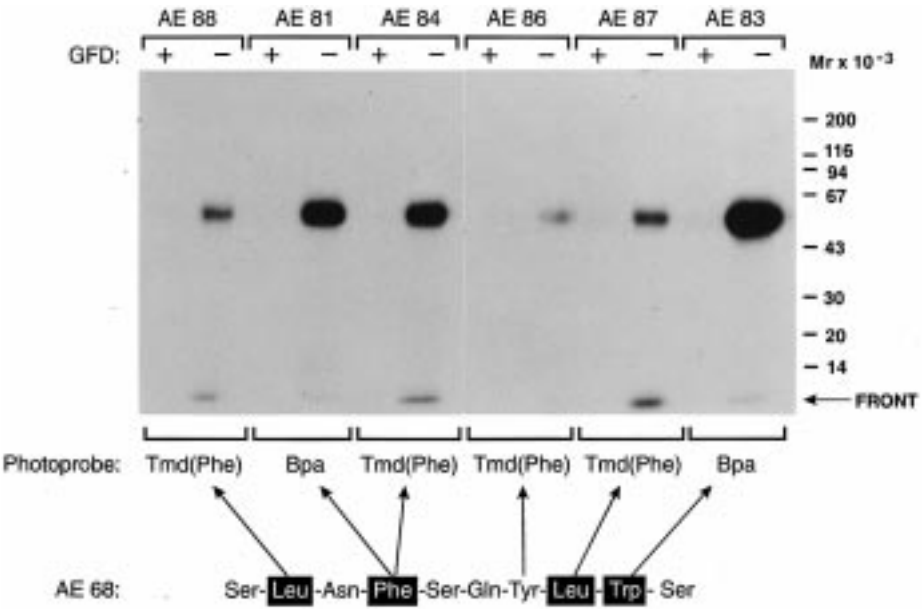

FIGURE 6: Specificity of the photoaffinity scanning analysis of uPAR probed by ligand competition experiments. Purified suPAR (5 μM) was preincubated with either buffer or GFD (10 μM) for 10 min before addition of the photoactivatable analogues of AE68 (5 μM) and subsequent photolysis for 45 min on ice. Samples were tested by SDS-polyacrylamide gel electrophoresis (12%), and the corresponding autoradiogram is shown.

by displacement of the preferred target residue in uPAR domains II + III just beyond the range of the photoprobe.

Proteolytic Domain Assignment of the Peptide Interaction Site in uPAR As Revealed by Photoaffinity Cross-Linking. Having demonstrated the specificity of the photoaffinity labeling of suPAR with analogues of AE68, we next attempted a gross topological domain mapping of the receptor interaction site for these peptide antagonists. Covalently linked [^{125}I]peptide·suPAR photoadducts were subjected to limited proteolysis using chymotrypsin, which preferentially cleaves the Tyr^{87}−Ser^{88} peptide bond, situated in the linker region between domain I and domain II, thereby liberating the NH_2-terminal domain I from the remaining domains II + III (*18, 19*). When Phe^4 in the peptide antagonist was replaced with either Bpa or Tmd(Phe), the major target for the photochemical insertion reaction is uPAR domain I, as in shown Figure 8. By contrast, replacement of Trp^9 with Bpa renders domains II + III of uPAR the exclusive target

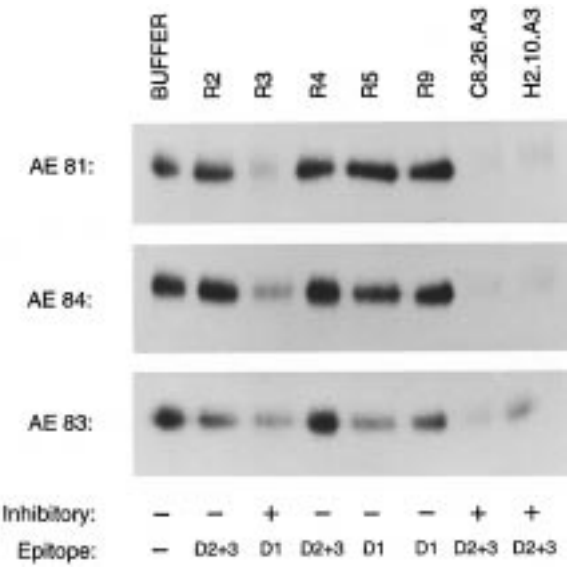

FIGURE 7: Inhibition of photoaffinity labeling by anti-uPAR monoclonal antibodies. Purified suPAR (5 μM) was preincubated for 10 min with an equimolar amount of the following murine monoclonal anti-uPAR antibodies (R2, R3, R4, R5, R9, C8.26A3, and H2.10A3) before addition of 5 μM AE81, AE83 or AE84. These samples were then subjected to photolysis on ice for 45 min before they were subjected to SDS−PAGE (without prior reduction or alkylation of samples). The corresponding autoradiograms are shown along with some functional properties determined for these monoclonal anti-uPAR antibodies, including their competitive inhibitory potential of the uPA−uPAR interaction and a gross topological domain assignment of their epitopes. Note that R5 is a weak, noncompetitive inhibitor of the uPA−uPAR interaction (*40*).

for the photochemical insertion. A further domain mapping of the labeled domains II + III by a preferred interdomain cleavage using pepsin (*30*) proved unsuccessful due to internal cleavages of the cross linked peptide antagonist, with the subsequent loss of the ^{125}I-labeled tag from the NH_2-terminus of AE83.

One of the important hallmarks of the high-affinity uPA−uPAR interaction is its absolute requirement for the integrity of the multidomain state of the receptor (*25*). A similar dependence on uPAR integrity also exists for the efficacy of the photoincorporation of ^{125}I-labeled peptide antagonist, since a preformed chymotrypsin-generated mixture of suPAR domain I and domains II + III exhibited very low photochemical cross-linking yields compared to a preparation of intact suPAR photolyzed in parallel (as demonstrated for AE84 in Figure 9). Similar results were obtained for AE81 and AE83.

DISCUSSION

Topological mapping of receptor−ligand interfaces by site-directed photoaffinity labeling represents an attractive, alternative research tool for structural investigations of protein−protein interactions, when the three-dimensional structures of such complexes have not been solved by NMR or X-ray crystallography (*41*−*43*). Since the three-dimensional structure of neither uPAR nor uPA−uPAR complexes have been solved experimentally, we have initiated a characterization of the ligand-interaction site in human uPAR using site-directed photoaffinity labeling. In the present study, we have explored the possibility of using a 15-mer peptide antagonist of the uPA−uPAR interaction, originally identified by bacteriophage display technology (*31*), as a potential probe for such a topological photoaffinity scanning analysis of the ligand-binding site in uPAR. This peptide was considered ideally suited for this purpose for the following reasons: First, it is an efficient competitive inhibitor of the uPA−uPAR interaction ($K_d \approx 9.5$ nM). Second, several of the properties of uPA inherent to its interaction with uPAR are shared by this peptide. These properties include the absolute requirement for the multidomain state of uPAR for a high-affinity interaction (Figure 9 and refs 25, 30), the ability of the ligand to titrate the uPAR-mediated enhancement of ANS fluorescence (Figure 2 and ref *25*), and the species specificity of the interaction, since no interaction with murine uPAR was observed (unpublished data). Third, residues in the peptide antagonist essential for uPAR binding were readily identified by alanine replacement experiments (Figures 3 and 4) and include the aromatic residues Phe and Trp. Such physiochemical properties of the ligand are in agreement with previous findings showing that a surface-exposed hydrophobic/aromatic patch in uPAR is involved in the interaction with distinct hydrophobic/aromatic amino acid side chains (Tyr, Phe, Ile, and Trp) in the ω-loop of GFD in uPA (*25*, *28*, *29*). Finally, the introduction of photoprobes into this linear peptide is conveniently accomplished by standard peptide synthesis techniques. The peptide antagonist was made photosensitive by incorporation of photochemically active derivatives of Phe (Tmd(Phe) or Bpa). These photophores exhibit different photochemistries (Figure 10A and ref *44*) and are comparable in size and hydrophobicity to the side chains of Phe and Trp.

By sequence comparison the consensus sequence X**F**XX-**YLW** was derived for the uPAR binding peptide antagonists originally identified by phage display technology (*31*). No sequence similarity to either uPA or uPAR was recognized in that report. However, a manual sequence alignment of the truncated peptide antagonist (AE68) and the relevant region of GFD in uPA reveals certain noticeable sequence similarities (Figure 10B). In particular, the occurrence of equally spaced Phe and Trp residues appears important, since these are among the essential structures for the receptor-binding properties of both ligands. The functional relevance of this shared motif is further substantiated by the experimental finding that insertion of either Gly or β-Ala between these two residues cannot be tolerated in a synthetic peptide without loss of antagonist function (data not shown). It is therefore likely that both ligands have the same binding site in uPAR with coinciding receptor−ligand interfaces.

The present site-directed affinity labeling of uPAR by photoinsertion of a peptide antagonist clearly reveals the composite nature of the ligand-binding site in uPAR, as illustrated in Figure 10B. Although separated by only four amino acids, Phe^4 and Trp^9 of the antagonist specifically interact with uPAR domain I and uPAR domains II + III, respectively. Binding of the small decapeptide ligand is therefore governed by its interaction with a complex binding site in uPAR containing structural elements remote in the primary sequence. Assembly of such a composite ligand interaction site in uPAR requires the spatial proximity of domain I with either domains II or III. This relationship therefore provides a rational structure−functional basis for the loss of the high affinity binding to uPA observed upon

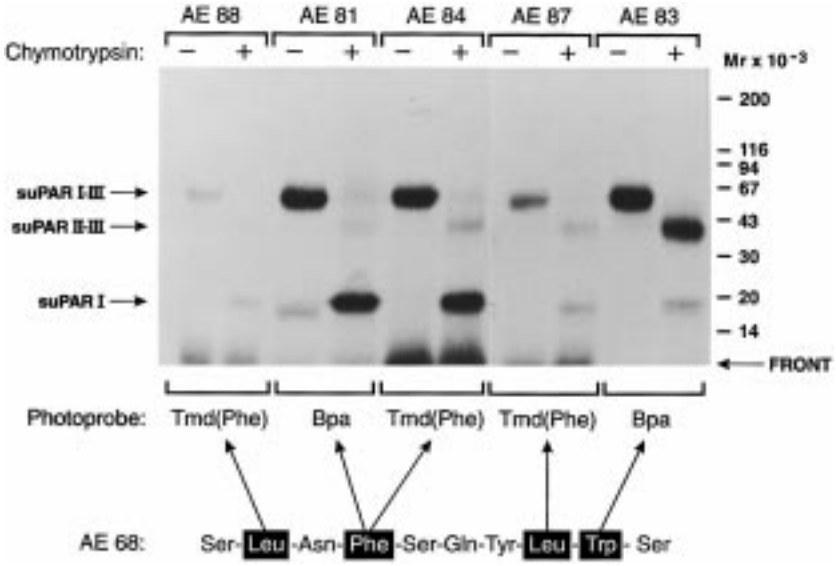

FIGURE 8: Domain assignment of photoincorporation of the peptide-binding antagonist. Purified suPAR was initially photolabeled with various analogues of AE68, as described in the legend to Figure 5. An aliquot from each was subsequently incubated for 90 min at 37 °C with chymotrypsin [E/S ≈ 1:2500 (w/w)]. The enzymatic cleavage was terminated by addition of 2 mM PMSF. Shown is the autoradiogram corresponding to a polyacrylamide gel (12%) subjected to SDS− PAGE after application of the photolyzed samples (reduced and alkylated). The mobilities of intact $suPAR_{1-277}$ (suPAR I−III), domain II + III_{88-277} (suPAR II−III), and domain I_{1-87} (suPAR I) are indicated by arrows.

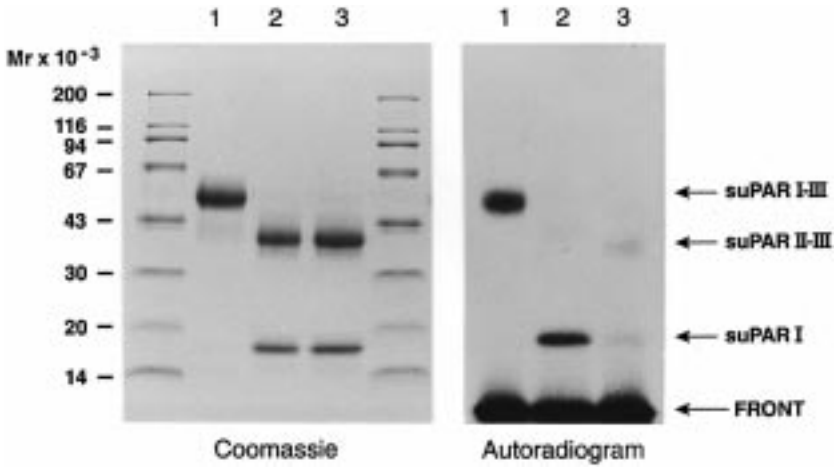

FIGURE 9: Intact uPAR is required for high-efficiency photolabeling. One aliquot of purified suPAR was initially treated with chymotrypsin [E/S ≈ 1:2500 (w/w)] for 90 min at 37 °C before addition of 2 mM PMSF to generate a mixture of suPAR domain I and domains II + III. Preparations of intact suPAR and chymotrypsin-treated suPAR subsequently received an equimolar amount (5 μM) of the photochemically active antagonist AE84. Photolysis proceeded for 45 min on ice. One aliquot of photolabeled intact suPAR was treated with chymotrypsin as described above. These preparations were then subjected to SDS−PAGE followed by autoradiography. Key: Lane 1, intact, photolabeled suPAR; lane 2, intact, photolabeled suPAR treated with chymotrypsin; lane 3, chymotrypsin-treated suPAR subsequently subjected to photolabeling.

enzymatic cleavage of interdomain linker sequences in the intact, multidomain uPAR (*25*, *30*). The occurrence of interdomain interactions within intact uPAR has previously been proposed on the basis of elution profiles from size-exclusion chromatography of chymotrypsin-treated suPAR, which reveal a reduced retention time for a certain population of uPAR domain I, suggesting a weak, noncovalent association with domains II + III (*19*). Certain single domain members of the Ly6/uPAR protein family have been shown to exhibit homophilic interdomain interactions, since the three-dimensional structures solved for some its members (*e.g.*, κ-bungarotoxin, α-cobratoxin, and cardiotoxin V) reveal extensive protein dimerization due to intermolecular hydrogen bonding between their central β-sheets (*45*−*47*).

The critical role of uPAR domain I in the binding of uPA is well established (*18*, *25*, *30*, *36*). A more confined localization of the ligand interaction site within uPAR domain I was recently obtained by "protein−protein footprinting" analysis, directly demonstrating the engagement of Tyr^{57} in formation of the receptor−ligand interface (*28*). An additional involvement of structures outside uPAR domain I in uPA binding has been suggested by enzymatic dissection of a covalent conjugate between ATF and suPAR formed by zero-length cross-linking, which demonstrates a weak, but distinct, cross-linking potential toward uPAR domains II + III (*30*). In the present study, we find a prominent and equal photoaffinity labeling of uPAR domain I and domains II + III, despite the latter having no detectable affinity for

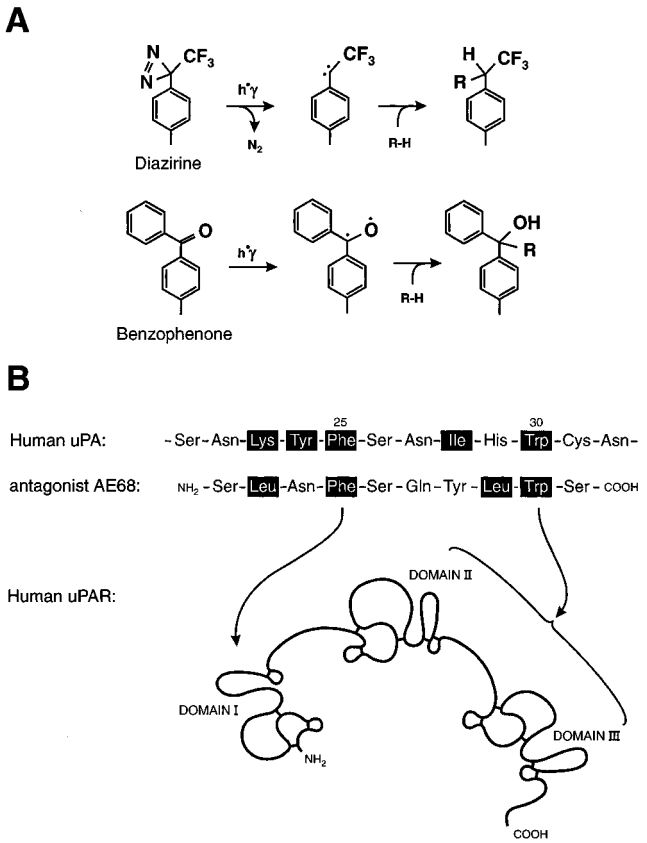

FIGURE 10: Photochemistry of the active photophores of Bpa and Tmd(Phe) and a schematic representation of the domain assignment in uPAR of the obtained photolabeling. Panel A: Excitation (~350 nM) of benzophenone (Bpa) generates a $n \rightarrow \pi^*$ biradical triplet state, which in aqueous solutions preferentially abstracts hydrogens from appropriately oriented C−H bonds of targent proteins compared to O−H of the solvent (*42*). In the absence of any preferred H-donors the maximal radius of the photochemical insertion reaction was calculated to 3.1 Å (centered on the ketone oxygen) before the biradical triplet would relax to the ground state. In contrast, excitation of trifluoromethyldiazirine (Tmd(Phe)) generates a highly reactive singlet carbene through an irreversible photodissociative process. The electrophilic nature of this intermediate renders solvent O−H bonds appropriate H- donors, thereby limiting the radius of the photochemical insertion reaction compared to Bpa (*44*). Specific labeling by Tmd(Phe) would therefore per se suggest a closer proximity between target protein and the photoprobe. Panel B: Alignment of the primary sequences of the truncated peptide antagonist (AE68) and a defined region of the ω-loop in GFD of human uPA involved in receptor binding is shown. The key functional residues of each ligand are highlighted (*28*, *29*). Domain assignments of the photolabeling of uPAR by photoprobes situated at the two prime positions in the antagonist are shown in a schematic two-dimensional model of uPAR (*19*, *20*).

uPA as an isolated fragment. By virtue of the short range of the photochemical insertion reaction, Phe[4] and Trp[9] in the peptide antagonist are shown to be directly associated with structures in uPAR domain I and domains II + III, respectively. Theoretical considerations supported by experimental findings define a maximal distance of 3.1 Å from the photoprobe to the abstractable hydrogen atom in the target protein (*42*). A future structural determination of the actual sites of the specific photoinsertion in uPAR, obtained in the present study by photoprobes replacing Phe[4] and Trp[9] in the peptide antagonist, will therefore increase our knowledge on the topology of the composite ligand binding site in uPAR and may also provide the rational basis for a detailed site-directed mutagenesis analysis of this binding site.

ACKNOWLEDGMENT

We would like to thank the following persons for their generous gift of purified reagent: Drs. Andrew Mazar and Jack Henkin (Abbott Laboratories, IL), Dr. Derek Saunders (Grünenthal, Germany) as well as Drs. Ulrich Weidle and Christiane Hartle (Boehringer Mannheim, Germany). Dr. Per Nielsen (NOVO-Nordisk, Denmark) is thanked for the performance of ESI-MS of purified peptides. The critical comments of Dr. Vincent Ellis (Thrombosis Research Institute, London, U.K.) on the manuscript are greatly appreciated as is the advice from Dr. Eicke Hoffmann (Boehringer Mannheim, Germany) regarding synthesis of Tmd-(Phe). The technical assistance of Helle Hymøller Hald, Charlotte Holm, and John Post is also greatly acknowledged.

REFERENCES

1. Collen, D., and Lijnen, H. R. (1994) in *The molecular Basis of Blood Diseases* (Stamatoyannopoulos, G. S., Nienhuis, A. W., Majerus, P. W., Varmus, H., Eds.) pp 725−752, WB Saunders Co., Philadelphia, PA.
2. Danø, K., Behrendt, N., Brünner, N., Ellis, V., Ploug, M., and Pyke, C. (1994) *Fibrinolysis 8*, Suppl. 1, 189−203.
3. Rømer, J., Bugge, T., Pyke, C., Lund, L. R., Flick, M. J., Degen, J., and Danø, K. (1996) *Nature Med. 2*, 287−292.
4. Vassalli, J. D., Baccini, D., and Belin, D. (1985) *J. Cell Biol. 100*, 86−92.
5. Plesner, T., Ploug, M., Ellis, V., Høyer-Hansen, G., Wittrup, M., Pedersen, T. L., Tscherning, T., Danø, K., and Hansen, N. E. (1994) *Blood 83*, 808−815.
6. Rømer, J., Lund, L. R., Eriksen, J., Pyke, C., Kristensen, P., and Danø, K. (1994) *Invest. Dermatol. 102*, 519−52.
7. Pyke, C., Ralfkiær, P., Rønne, E., Høyer-Hansen, G., Kirkeby, G. (1994) *Histopathology 24*, 131−138.
8. Ellis, V., Ploug, M., Plesner, T., and Danø K. (1995) in *Fibrinolysis in Disease* (Glass-Greenwalt, P., Ed.) pp 30−42, CRC Press, New York.
9. Mignatti, P., Robbins, E., and Rifkin, D. B. (1986) *Cell 47*, 487−498.
10. Ossowski, L. (1988) *J. Cell Biol. 107*, 2437−2445.
11. Ossowski, L., Russo-Payne, H and Wilson, E. L. (1991) *Cancer Res. 51*, 274−281 .
12. Crowley, W. C., Choen, R. L., Lucas, B. K., Liu, M. A., Shuman, M. A., and Levinson, A. D. (1993) *Proc. Natl. Acad. Sci. U.S.A.* 90, 5021−5025.
13. Kook, Y.-H., Adamski, J., Zelent, A., and Ossowski, L. (1994) *EMBO J. 13*, 3983−3991.
14. Min, H. Y., Doyle, L. V., Vitt, C. R., Zandonella, C. L., Stratton-Thomas, J. R., Shuman, M. A., and Rosenberg, S. (1996) *Cancer Res. 56*, 2428−2433.
15. Yu, W., Kim, J., and Ossowski, L. (1997) *J. Cell Biol. 137*, 767−770.
16. Roldan, A. L., Cubellis, M. V., Mascucci, M. T., Behrendt, N., Lund, L. R., Danø, K., Appella, E., and Blasi, F. (1990) *EMBO J. 9*, 467−474.
17. Ploug, M., Rønne, E., Behrendt, N., Jensen, A., Blasi, F., and Danø, K. (1991) *J. Biol. Chem. 266*, 1926−1936.
18. Behrendt, N., Ploug, M., Patthy, L., Houen, G., Blasi, F., and Danø, K. (1991) *J. Biol. Chem. 266*, 7842−7847.
19. Ploug, M., Kjalke, M., Rønne, E., Weidle, U., Høyer-Hansen, G., and Danø, K. (1993) *Biol. Chem. 268*, 17539−17546.
20. Ploug, M., and Ellis, V. (1994) *FEBS Lett. 349*, 163−168.
21. Kieffer, B., Driscoll, P. C., Campbell, I. D., Willis, A. C., van der Merve, P. A., and Davis, S. J. (1994) *Biochemistry 33*, 4471−4482.
22. Fletcher, C. M., Harrison, R. A., Lachmann, P. J., and Neuhaus, D. (1994) *Structure 2*, 185−199.

23. Ploug, M., Eriksen, J., Plesner, T., Hansen, N. E., and Danø, K. (1992) *Eur. J. Biochem. 208*, 397−404.
24. Ploug, M., Plesner, T., Rønne, E., Ellis, V., Høyer-Hansen, G., Hansen, N. E., and Danø, K. (1992) *Blood 79*, 1447−1455.
25. Ploug, M., Ellis, V., and Danø, K. (1994) *Biochemistry 33*, 8991−8997.
26. Appella, E., Robinson, E. A., Ullrich, S. J., Stoppelli, M. P., Corti, A., Cassani, G., and Blasi, F. (1987) *J. Biol. Chem. 262*, 4437−4440.
27. Hansen, A. P., Petros, A. M., Meadows, R. P., Nettesheim, D. G., Mazar, A. P., Olejniczak, E. T., Pederson, T. M., Henkin, J., and Fesik, S. (1994) *Biochemistry 33*, 4847−4864.
28. Ploug, M., Rahbek-Nielsen, H., Ellis, V., Roepstorff, P., and Danø, K. (1995) *Biochemistry 34*, 12524−12534.
29. Magdolen, V., Rettenberger, P., Koppitz, M., Goretzki, L., Kessler, H., Weidle, U., König, B., Graeff, H., Schmitt, M., and Wilhelm, O (1996) *Eur. J. Biochem. 237*, 743−751.
30. Behrendt, N., Rønne, E., and Danø, K. (1996) *J. Biol. Chem. 271*, 22885−22894.
31. Goodson, R. J., Doyle, M. V., Kaufman, S. E., and Rosenberg, S. (1994) *Proc. Natl. Acad. Sci. U.S.A.* 91, 7129−7133.
32. Nassal, M (1984) *J. Am. Chem. Soc. 106*, 7540−7545.
33. Shih, L. B., and Bayley, H. (1985) *Anal. Biochem. 144*, 132−141.
34. Delfino, J. M., Schreiber, S. L., and Richards, F. M. (1993) *J. Am. Chem. Soc. 115*, 3458−3474.
35. Falchetto, R., Vorherr, T., Brunner, J., and Carafoli, E. (1991) *J. Biol. Chem. 266*, 2930−2036.
36. Rønne, E., Behrendt, N., Ellis, V., Ploug, M., Danø, K., and Høyer-Hansen, G. (1991) *FEBS Lett. 288*, 233−236.
37. Karlsson, R., Michaelsson, A., and Mattson, A. (1991) *J. Immunol. Methods 145*, 229−240.
38. Nielsen, L. S., Kellerman, G. M., Behrendt, N., Picone, R., Danø, K., and Blasi, F. (1988) *J. Biol. Chem. 263*, 2358−2363.
39. Laemmli, U.K. (1970) *Nature 227*, 680−685.
40. List, K., Høyer-Hansen, G., Rønne, E., Danø, K., and Behrendt, N. (1997) *Fibrinolysis Proteolysis 11* (Suppl. 3), 50 (abstract).
41. Brunner, J. (1993) *Annu. Rev. Biochem. 62*, 483−514.
42. Dormán, G., and Prestwich, G. D. (1994) *Biochemistry 33*, 5661−5673.
43. Kotzyba-Hibert, F., Kapfer, I., and Goeldner, M. (1995) *Angew. Chem., Int. Ed. Engl. 34*, 1296−1312.
44. Weber, P. J. A., and Beck-Sickinger, A. G. (1997) *J. Peptide Res. 49*, 375−383.
45. Dewan, J. C., Grant, G. A., and Sacchettini, J. C. (1994) *Biochemistry 33*, 13147−13154.
46. Betzel, C., Lange, G., Pal, G. P., Wilson, K. S., Maelicke, A., and Saenger, W. (1991) *J. Biol. Chem. 266*, 21530−21536.
47. Sun, Y.-J., Wu, W.-G., Chiang, C.-H., Hsin, A.-Y., and Hsiao, C.-D (1997) *Biochemistry 36*, 2403−2413.

BI972787K